INTERNATIONAL JOURNAL OF CLIMATOLOGY
Int. J. Climatol. **37**: 2765–2781 (2017)
Published online 4 September 2016 in Wiley Online Library
(wileyonlinelibrary.com) DOI: 10.1002/joc.4878

RMetS
Royal Meteorological Society

Future change in the frequency and intensity of wintertime North Pacific blocking in CMIP5 models

Doo Young Lee[a] and Joong-Bae Ahn[b]*
[a] *Earth Sciences Department, Barcelona Supercomputing Center, Spain*
[b] *Pusan National University, Busan, Republic of Korea*

ABSTRACT: The current status and future changes in the frequency and intensity of climatological blocking activity over the North Pacific region are investigated using historical and two Representative Concentration Pathway (RCP4.5 and 8.5) simulations in the coupled climate models from phase 5 of the Coupled Model Intercomparison Project (CMIP5) for boreal winters (December–February) over a 30-year period. The future change in the Pacific blocking frequency and intensity are examined in terms of the projected meridional thickness gradient, Hadley circulation changes, and changes in the probability distribution of categorized blocking strength. The five CMIP5 models that show better performance in reproducing climatological blocking events in the historical simulations for the Pacific region are selected for the analyses of the projected blocking activities. The climatological winter Pacific blocking frequencies of most of the individual models and model mean values show a tendency to decrease under global warming conditions. The trend is closely linked with the strong upper level westerly wind, resulting in less meandering air flow, consistent with the enhanced meridional temperature gradients at mid-latitude in the future climate. The decreased frequency in climatological atmospheric blocking over the Pacific under warming may also be influenced by the strengthening of the north–south temperature gradients due to the poleward extension of Hadley circulation in the subtropics. The climatology of the Pacific blocking intensity in boreal winter also tends to decrease slightly due to a future reduction in the number of strong blocking events.

KEY WORDS blocking frequency; blocking intensity; Pacific blocking; CMIP5; Global warming; RCP

Received 29 October 2015; Revised 24 July 2016; Accepted 1 August 2016

1. Introduction

A general stagnation of weather/climate caused by atmospheric blocking known as a large-scale quasi-stationary extra-tropical flow regime can affect not only mid-latitude synoptic circulation but also extreme events, such as floods, heat waves, droughts, and cold waves (Tanaka and Milkovich, 1990; Black *et al*., 2004; Neiman *et al*., 2004; Buehler *et al*., 2011; Dole *et al*., 2011; Park *et al*., 2011), lasting for several days to even weeks. The typical blocking pattern is characterized by an upper tropospheric flow causing a temporary deflection of the regular west to east progression of weather systems in mid-latitude (Nakamura, 1994).

The climatological characteristics of blocking events, such as frequency and locations of occurrence, duration, and intensity, in the Northern Hemisphere have been described by many researchers (Rex, 1950; Triedl *et al*., 1981; Lejenas and Okland, 1983; Gruza and Korovkina, 1991; Tibaldi *et al*., 1994; Lupo and Smith, 1995; Wiedenmann *et al*., 2002). Generally, it was confirmed that blocking events in the Northern Hemisphere occur most frequently over the Pacific and Atlantic Oceans during the cold season and, additionally, that blocking events are stronger during the cold season over the ocean region than during the warm season over the continent.

Many studies (e.g. D'Andrea *et al*., 1998; Barriopedro *et al*., 2008; Matsueda *et al*., 2009; Scaife *et al*., 2010; Scaife *et al*., 2011; Vial and Osborn, 2012; Anstey *et al*., 2013; Berckmans *et al*., 2013; Dunn-Sigouin and Son, 2013; Masato *et al*., 2013) have revealed the existence of substantial model biases in simulating blocking due to various factors such as coarse spatial resolution, external forcing, and improper representation of physical processes and parameterization. Some studies (Matsueda *et al*., 2009; Scaife *et al*., 2010, 2011; Anstey *et al*., 2013) have tried to diagnostically correct the model mean bias to evaluate the blocking simulation.

It is important to project potential changes of blocking in many respects under global warming conditions. Recently, various research activities associated with the blocking events in the future climate have been carried out using the climate models (Matsueda *et al*., 2009; Barnes and Hartmann, 2010; Scaife *et al*., 2010; Barnes *et al*., 2012; Dunn-Sigouin and Son, 2013; Masato *et al*., 2013). Nevertheless, it is rather difficult to reliably determine the future change using the climate models, mainly due to the deficiency in performing historical simulation.

* Correspondence to: J.-B. Ahn, Department of Atmospheric Sciences, Pusan National University, 2, Busandaehak-ro 63beon-gil, Geumjeong-gu, Busan, 46241, Republic of Korea. E-mail: jbahn@pusan.ac.kr

Table 1. Description of the CMIP5 models used in the study.

No.	Model	Institute	Horizontal resolution
1	ACCESS1-0	Commonwealth Scientific and Industrial Research Organization and Bureau of Meteorology (CSIRO-BOM)	192 × 144 (1.875° × 1.25°)
2	ACCESS1-3	CSIRO-BOM	192 × 144 (1.875° × 1.25°)
3	BCC-CSM1-1	Beijing Climate Center (BCC)	128 × 64 (2.8125° × 2.8125°)
4	BCC-CSM1-1-M	BCC	320 × 160 (1.125° × 1.125°)
5	CanESM2	Canadian Centre for Climate Modelling and Analysis (CCCMA)	128 × 64 (2.8125° × 2.8125°)
6	CCSM4	NCAR	288 × 192 (1.25° × 0.9375°)
7	CMCC-CM	Centro Euro-Mediterraneo sui Cambiamenti Climatici	480 × 240 (0.75° × 0.75°)
8	CMCC-CMS	Centro Euro-Mediterraneo sui Cambiamenti Climatici	192 × 96 (1.875° × 1.875°)
9	CNRM-CM5	Centre National de Recherches Meteorologiques/Centre European de Recherche et Formation Avancees en Calcul Scientifique (CNRM-CERFACS)	256 × 128 (1.40625° × 1.40625°)
10	GFDL-CM3	NOAA Geophysical Fluid Dynamics Laboratory (NOAA GFDL)	144 × 90 (2.5° × 2.0°)
11	GFDL-ESM2G	NOAA GFDL	144 × 90 (2.5° × 2.0°)
12	GFDL-ESM2M	NOAA GFDL	144 × 90 (2.5° × 2.0°)
13	HadGEM2-CC	Met Office Hadley Centre (MOHC)	192 × 144 (1.875° × 1.25°)
14	IPSL-CM5A-LR	Institute Pierre-Simon Laplace (IPSL)	96 × 96 (3.75° × 1.875°)
15	IPSL-CM5A-MR	IPSL	144 × 143 (2.5° × 1.2676°)
16	IPSL-CM5B-LR	IPSL	96 × 96 (3.75° × 1.875°)
17	MIROC-ESM	Japan Agency for Marine-Earth Science and Technology, Atmosphere and Ocean Research Institute, and National Institute for Environmental Studies	128 × 64 (2.8125° × 2.8125°)
18	MIROC-ESM-CHEM	Japan Agency for Marine-Earth Science and Technology, Atmosphere and Ocean Research Institute, and National Institute for Environmental Studies	128 × 64 (2.8125° × 2.8125°)
19	MPI-ESM-LR	Max Planck Institute for Meteorology (MPI-M)	192 × 96 (1.875° × 1.875°)
20	MPI-ESM-MR	MPI-M	192 × 96 (1.875° × 1.875°)
21	MRI-CGCM3	Meteorological Research Institute (MRI)	320 × 160 (1.125° × 1.125°)
22	NorESM1-M	Norwegian Climate Centre (NCC)	144 × 96 (2.5° × 1.875°)

To overcome this limitation and generate more accurate and reliable future climate prediction, in this study, we first focus on the selection of models that show superior performance in simulating climatological winter blocking events in the historical simulations using statistical diagnostics and then use the outputs obtained from the selected individual models, as well as the mean of the individual models. This study investigates the current and future trends of the climatological blocking events in terms of frequency and intensity in the North Pacific region, using available historical (1975/1976–2004/2005) and Representative Concentration Pathway (RCP, 2070/2071-2099/2100) simulations during the Northern Hemisphere winter (December–February, DJF) for a 30-year period obtained from the climate models in the Coupled Model Intercomparison Project Phase 5 (CMIP5, Taylor *et al*., 2012). Furthermore, we also examine the possible factors contributing to future change in the Pacific blocking frequency (BF) and intensity (BI) in terms of the trends of meridional thickness gradient in mid-latitude, Hadley circulation changes in subtropical region, and changes in the probability distribution of categorized blocking strength.

Section 2 presents a brief description of the observational data, coupled model data participating in the CMIP5, and methods used to measure the blocking activity in this study. Section 3 describes the performance of the CMIP5 models in wintertime Pacific blocking simulations. Sections 4 and 5 describe the future change of climatological BF and BI over the Pacific regions in CMIP5 models, respectively. The summary and conclusions are given in the final section.

2. Data and methodology

2.1. Data

The results of coupled general circulation models (CGCMs) that participated in CMIP5 (Taylor *et al*., 2012) are used in this study. The models are briefly described in Table 1. The models are selected by the availability of daily geopotential height and zonal wind data from the historical (1975/1976–2004/2005), RCP4.5 (2070/2071–2099/2100), and RCP8.5 (2070/2071–2099/2100) simulations for boreal winter (DJF) over a period of 30 years. The first ensemble member for each model is used.

The 20th century climate simulations that are referred to as the historical runs can be statistically compared with the twentieth century observations. The RCP4.5 runs assume that radiative forcing will increase and then stabilize at approximately 4.5 W m^{-2} (about 650 CO_2 equivalent concentrations) after 2100. The RCP8.5 runs are scenario simulations with a rapid warming, specifically with a high

radiative forcing pathway reaching >8.5 Wm^{-2} (more than about 1370 CO_2 equivalent concentrations) in 2100. These two future simulations representing a midrange mitigation and high emission scenario were chosen because they properly cover a broad range of plausible futures in terms of greenhouse gas emissions and their impacts on climate.

The National Centers for Atmospheric Prediction (NCEP) and the National Center for Atmospheric Research (NCAR) reanalysis with a $2.5^\circ \times 2.5^\circ$ resolution is used as an observational dataset (Kalnay *et al*., 1996). To estimate the change of blocking activity between early and the recent 30 years of observation, we utilize 60 winters (DJF) during the period 1954/1955–2013/2014. In order to evaluate the performance of the CMIP5 models, reanalysis data from the same period as the historical runs (1975/1976–2004/2005) is also used.

2.2. Blocking frequency

We adopt an objective blocking detection method defined as the value of the meridional gradient of the geopotential height at 500 hPa (Lejenas and Okland, 1983; Tibaldi and Molteni, 1990; Lupo and Smith, 1995; Wiedenmann *et al*., 2002; Barriopedro *et al*., 2006; You and Ahn, 2012; Park and Ahn, 2014).

For each longitude, the northern 500 hPa geopotential height gradient (GHGN) and the southern 500 hPa geopotential height gradient (GHGS) are computed as follows:

$$\mathrm{GHGN} = \frac{Z\left(\lambda, \phi_\mathrm{N}\right) - Z\left(\lambda, \phi_0\right)}{\phi_\mathrm{N} - \phi_0} \tag{1}$$

$$\mathrm{GHGS} = \frac{Z\left(\lambda, \phi_0\right) - Z\left(\lambda, \phi_\mathrm{s}\right)}{\phi_0 - \phi_\mathrm{S}}, \quad \phi_\mathrm{N} = 77.5^\circ + \Delta,$$
$$\phi_0 = 60.0^\circ + \Delta, \quad \phi_\mathrm{S} = 40.0^\circ + \Delta,$$
$$\Delta = -5^\circ, \ -2.5^\circ, \ 0^\circ, \ 2.5^\circ, \ 5^\circ \tag{2}$$

where $Z(\lambda, \phi)$ means the 500 hPa geopotential height at longitude (λ) and latitude (ϕ).

A given longitude is said to be blocked as an instantaneous blocking at a given time if the following two conditions are satisfied for at least one value of Δ.

$$\mathrm{GHGN} < -10 \ \mathrm{m} \ {}^\circ\mathrm{latitude}^{-1}, \text{ and } \mathrm{GHGS} > 0$$

Furthermore, a persistent blocking event is defined as occurring when an instantaneous blocking event lasts at least 5 consecutive days at a grid point. BF is defined as the percentage ratio of the number of persistent blocking days to the number of days in winter (90 days).

2.3. Blocking intensity

Before applying the procedures for BI suggested by Wiedenmann *et al.* (2002), we first detect a blocking region where there are at least five consecutive blocking grid points on 1 day. Within this blocking region, we find the longitude λ_c at which the maximum value of the 500 hPa geopotential height occurs. The maximum 500 hPa geopotential height in the blocking region is defined as a blocking central height, $Z(\lambda_\mathrm{c}, \phi)$, at the longitude ($\lambda_\mathrm{c}$) and latitude ($\phi$).

The BI index for the blocking region is calculated by normalizing the central height value $Z(\lambda_\mathrm{c}, \phi)$ with a reference contour (RC) line.

$$\mathrm{BI} = 100 \left[\frac{Z\left(\lambda_\mathrm{c}, \ \phi\right)}{\mathrm{RC}} - 1.0\right] \tag{3}$$

RC is obtained by averaging the upstream $Z(\lambda_\mathrm{u}, \phi)$ and downstream $Z(\lambda_\mathrm{d}, \phi)$ heights located at the same latitude as the blocking centre, with the central height $Z(\lambda_\mathrm{c}, \phi)$.

$$\mathrm{RC} = \left[\frac{\left(\frac{Z(\lambda_\mathrm{u}, \ \phi)+Z(\lambda_\mathrm{c}, \ \phi)}{2}\right) + \left(\frac{Z(\lambda_\mathrm{d}, \ \phi)+Z(\lambda_\mathrm{c}, \ \phi)}{2}\right)}{2}\right] \tag{4}$$

The λ_u and λ_d values are fixed to 10° westward and eastward of the half-extension from the blocking centre, respectively (Barriopedro *et al*., 2006; Cheung *et al*., 2013).

3. Assessment of the capability of CMIP5 models in blocking simulation and model selection

3.1. BFs in the CMIP5 models

To examine the change of BF for the present and future climates in observation and model simulations, we first evaluate the blocking activity of the 22 CMIP5 CGCMs and of observations over the Northern Hemisphere during DJF (Figure 1). Figure 1(a) shows the longitudinal distribution of climatological DJF BFs for the early (1954/1955–1983/1984) and the recent (1984/1985–2013/2014) 30 years from NCEP/NCAR reanalysis datasets. Two main sectors of blocking are readily identifiable over the European continent-northeastern Atlantic Ocean (Euro-Atlantic sector) and the North Pacific Ocean (Pacific sector), as already noted by many earlier studies (D'Andrea *et al*., 1998; Barriopedro *et al*., 2006; Matsueda *et al*., 2009; Cheung *et al*., 2013). Although the Euro-Atlantic sector in observation for both periods shows the highest BF with a dominant peak, the change in BF between the two periods, especially near the dateline, over the Pacific sector is more pronounced and much larger than that over the Euro-Atlantic sector (Figure 1(a)). In the model mean (the average of climatological BFs of each model; Figure 1(b)), the major climatological features of the BF of historical simulation are very similar to those of observations over the Pacific sector, while unrealistically low BF occurs over the Euro-Atlantic sector. Based on these results, implying that many CMIP5 models struggle to simulate blocking in the Euro-Atlantic sector, we henceforth focus on the Pacific sector as the target area of this research related to the changes of blocking activity.

In fact, it is not easy to ascertain clear causation between the change in the observed BF over the Pacific sector and the observed radiative forcings or internal variabilities.

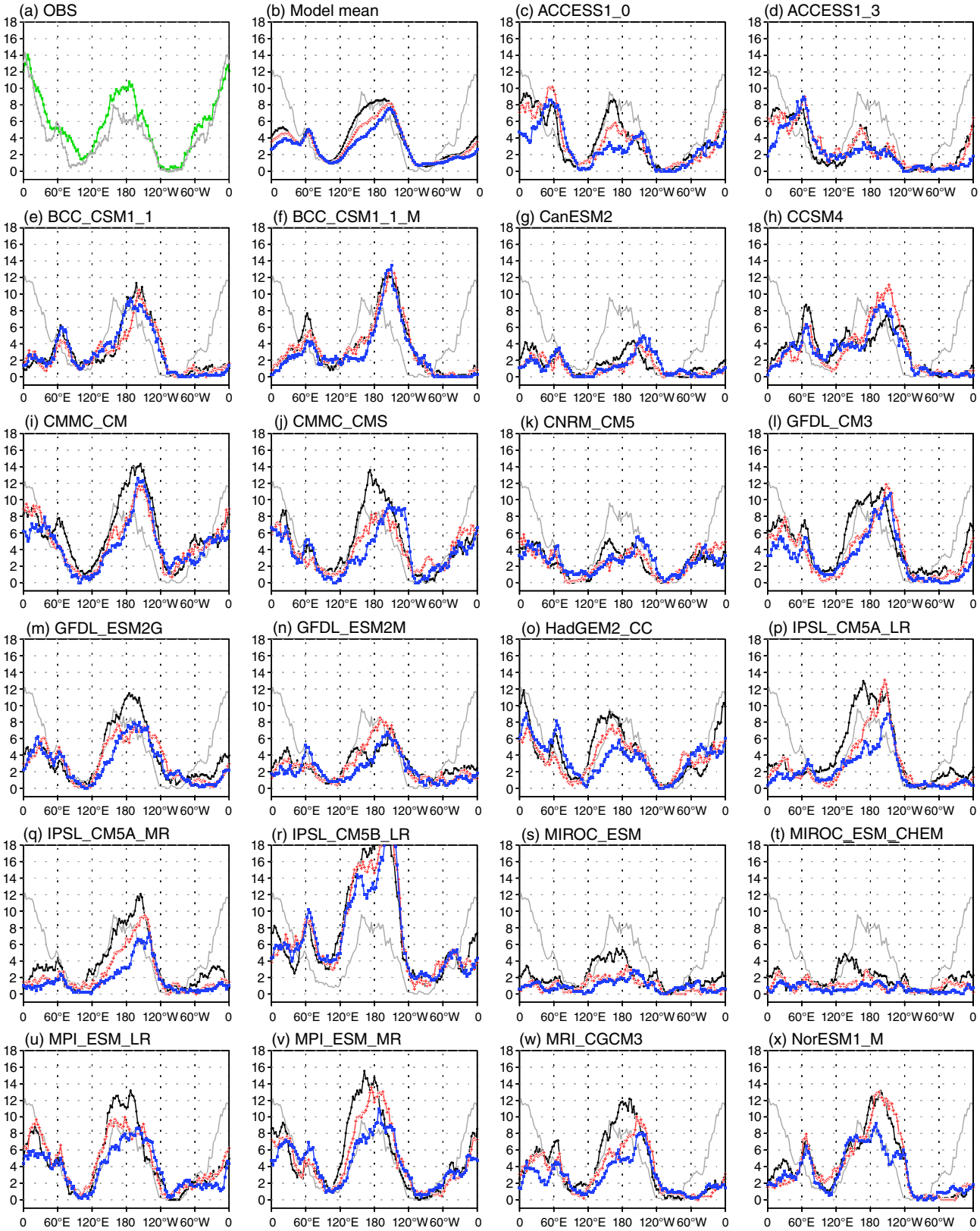

Figure 1. Climatology of boreal winter (December through February, DJF) BF (unit: %) as a function of longitude for (a) observation (green: 1954/1955–1983/1984, grey: 1984/1985–2013/2014) and the (b) model mean as the average of climatological BFs of each model and (c–x) individual models in the three CMIP5 experiments that consist of the historical (black: 1975/1976–2004/2005), RCP4.5 (red: 2070/2071–2099/2100) and RCP8.5 (blue: 2070/2071–2099/2100) simulations, respectively. The grey lines in (b–x) represent the observation for the same period (1975/1976–2004/2005) as historical simulation for a fair comparison. [Colour figure can be viewed at wileyonlinelibrary.com].

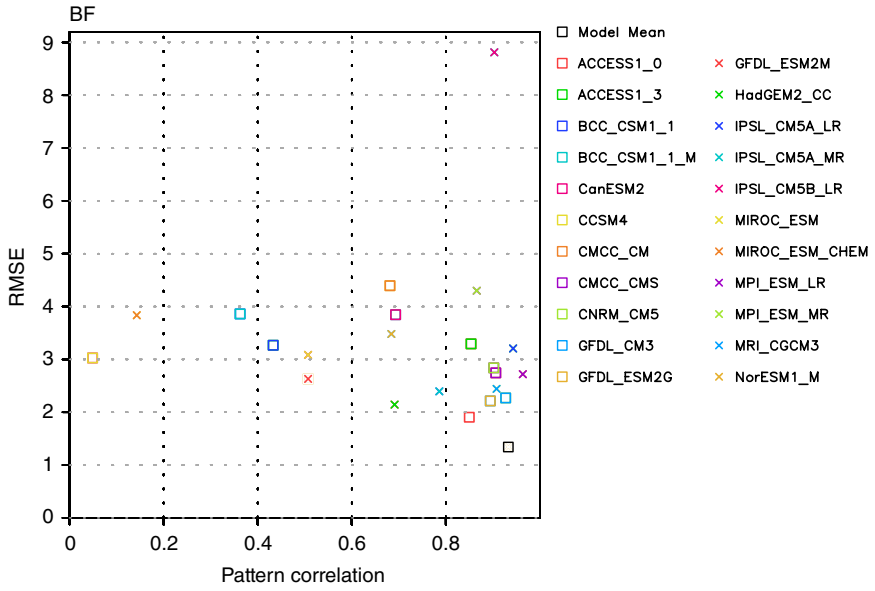

Figure 2. Scatter diagram between the spatial PCCs and RMSEs (unit: %) for climatological blocking frequencies (BFs) over the Pacific sector (110°E–120°W) derived from each model and its model mean in the historical (1975/1976–2004/2005) CMIP5 scenario. [Colour figure can be viewed at wileyonlinelibrary.com].

Furthermore, all models having inherent bias, and errors do not reflect a consistent trend in the change of BF. Nevertheless, our approach considers a possible potential link between the effect of radiative forcing under global warming and the change of BF, using a long period of data to reduce the influence of internal variability (Dunn-Sigouin and Son, 2013).

In the historical simulations, we can find that the phase, shape, and amplitude of the BF for some models, such as ACCESS1_0, GFDL_CM3, GFDL_ESM2G, and HadGEM2_CC, over the Pacific sector are well reproduced. ACCESS1_3, CanESM2, CNRM_CM5, and two MIROC models tend to underestimate the frequency of Pacific blocking, while the BFs of CMCC_CM, IPSL_CM5B_LR, and MPI_ESM_MR highly overestimate amplitude in the Pacific area. In the future climates under the RCP4.5 and RCP8.5 simulations, the North Pacific BF of the model mean clearly shows a decreasing tendency compared to the historical simulation, while it is rather difficult to see a similar trend to the model mean in the following eight models: ACCESS1_3, two BCC_CSM1s, CanESM2, CCSM4, CNRM_CM5, GFDL_ESM2M, and NorESM1_M. The significant future decrease in the Pacific BF for most of the models, as well as the model mean, is apparent in the western part of the peak of the BF in the historical simulations. Using the difference between the 500 hPa geopotential height at two latitudes and specified criteria to detect the blocking characteristics, Mokhov *et al*. (2014) show the decrease of wintertime BF in the Northern Hemisphere as a whole, in spite of the increase of BF in the Euro-Atlantic sector during winter under the RCP scenarios. This finding supports our results that the wintertime BF over the Pacific sector, as one of two main blocking sectors in the Northern Hemisphere, generally has a decreasing trend under future global warming.

To select the models suitable for dealing with the future change of wintertime BF among the various CMIP5 models, the historical CMIP5 simulation performance of each model is investigated in terms of the BF over the Pacific region. For this purpose, we examined the similarity in the patterns of change between the model (or multi-model mean) and observation. The spatial pattern correlation coefficients (PCC; Jolliffe and Stephenson, 2003; World Meteorological Organization, 2006) between the anomalies of the observed and model-simulated pattern are calculated. The root mean square errors (RMSEs; Jolliffe and Stephenson, 2003; World Meteorological Organization, 2006), showing the difference between the simulated and observed fields, as a measure of the accuracy of the model compared with observation are also computed. Figure 2 illustrates the scatter diagram between the spatial PCCs and RMSEs for climatological BFs in the Pacific sector (110°E–120°W) obtained from the individual models in historical (1975/1976–2004/2005) CMIP5 simulations and the model mean of the BFs. The PCC and RMSE results are presented in Table 2. While the PCC skills of climatological BFs obtained by the CCSM4, CMCC_CM, and two BCC_CSM1 models tend to perform relatively poorly compared to those by the other models, the skills from the MPI_ESM_LR, IPSL_CM5A_LR, and GFDL_CM3 model simulations indicate very high performances of >0.92, significant at the 98% confidence level from a two-tailed Student's *t* test. The RMSE of the BFs between the historical simulation and observation shows that six of the models, ACCESS1_0, GFDL_CM3, GFDL_ESM2G, HadGEM2_CC, IPSL_CM5A_MR, and MRI_CGCM3, have lower errors (<∼2.5) than the other models. The PCC and RMSE for the model mean show significantly higher skill (∼0.93) and relatively lower error (∼1.34) than those for the individual models. Ten out of the 22 CMIP5 models are classified as 'good performing'

models, of which PCC and RMSE are larger and smaller than the average of total PCCs (0.7) and RMSEs (3.306), respectively.

3.2. Blocking pattern of the CMIP5 models

To obtain an optimal representation of the spatial pattern of BF during boreal winter, we decompose the geopotential height anomaly at 500 hPa into empirical orthogonal function (EOF) modes after linearly detrending the individual CMIP5 historical simulations and observed data over the Pacific sector (110°E–120°W, 20°–75°N) during DJF for the period of 30 years (1975/1976–2004/2005). We then compute the temporal correlation coefficients (TCCs) between the wintertime BFs, defined as the zonally averaged BF over the Pacific blocking sector (110°E–120°W) for the period of 30 years, and principal component (PC) time series of the EOF leading modes for each model and observation (Table 3). Here, it is shown that the correlation coefficient between BF and EOF PC3 for observations (reanalysis) has a high value of about 0.768. Moreover, based on the time mean and ±1 S.D. of the zonally averaged wintertime BFs over the Pacific blocking sector, a composite anomaly field, obtained by combining positive and negative 500 hPa geopotential height anomaly fields that exceed ±1 S.D., respectively, and then subtracting the negative anomaly field from the positive one, is produced. The composite field is quite close to the spatial pattern of the EOF third mode (spatial pattern correlation is about 0.83, figure not shown), which indicates that the BF over the Pacific sector for boreal winter is significantly related to the third EOF mode of the 500 hPa geopotential height anomaly. You and Ahn (2012) also found the close relationship between the observed second EOF modes of geopotential height at 500 hPa and observed blocking field.

The EOF modes with the highest TCC between the BF and EOF PCs (Table 3) are shown in Figure 3. The spatial distribution for the observed blocking pattern over the North Pacific region has a meridional dipole structure: one centre located in the east of Japan, around 35°N, 160°E, and the other near the Bering Sea, around 60°N, 170°E. It is also shown that the blocking patterns of most models and model mean are similar to that of observation, despite the slight difference in the aspect of location and strength of the meridional dipole mode. Furthermore, to check the reproducibility of the structural characteristics of the observed blocking mode in the Pacific sector for each model, the spatial PCC between observation and individual models for the wintertime EOF blocking modes shown in Figure 3 is also illustrated in Table 4. The models that have a significant PCC skill score at the 90% confidence level from a two-tailed Student's *t* test are selected. The ACCESS1-3, BCC-CSM1-1-M, GFDL-ESM2G, and NorESM1-M model simulations exhibit relatively good skills, significant at the 95% confidence level from a *t*-test, while some model simulations such as CMCC-CMS and IPSL-CM5A-MR show relatively poor performance.

Through comparison of the major distinct features on the variability of climatological BFs in Table 2 of Section 3.1

Table 2. Spatial PCCs (and significance test) and RMSEs (unit: %) for climatological BFs over the Pacific sector (110°E–120°W) derived from each model and their model mean in the historical (1975/1976–2004/2005) simulations. The asterisk (*) superscript indicates the model, of which PCC and RMSE are larger and smaller than the average of total PCCs (0.7) and RMSEs (3.306), respectively.

	Model mean	ACCESS1-0* GFDL-ESM2M	ACCESS1-3* HadGEM2-CC	BCC-CSM1-1 IPSL-CM5A-LR*	BCC-CSM1-1-M IPSL-CM5A-MR*	CanESM2 IPSL-CM5B-LR	CCSM4 MIROC-ESM	CMCC-CM MIROC-ESM-CHEM	CMCC-CMS* MPI-ESM-LR*	CNRM-CM5* MPI-ESM-MR	GFDL-CM3* MRI-CGCM3*	GFDL-ESM2G* NorESM1-M
PCC (significance test)	0.933 (98%)	0.850 (95%)	0.854 (95%)	0.433 (75%)	0.363 (70%)	0.693 (85%)	0.049 (65%)	0.681 (85%)	0.906 (95%)	0.902 (95%)	0.927 (98%)	0.895 (95%)
		0.507 (80%)	0.691 (85%)	0.943 (98%)	0.786 (90%)	0.903 (95%)	0.507 (80%)	0.143 (65%)	0.964 (99%)	0.866 (95%)	0.908 (95%)	0.684 (85%)
RMSE	1.342	1.904	3.295	3.269	3.861	3.845	3.027	4.394	2.746	2.841	2.270	2.215
		2.630	2.144	3.207	2.395	8.812	3.086	3.836	2.721	4.301	2.442	3.481

Table 3. TCCs between BF and EOF PC time series of the detrended geopotential height anomaly at 500 hPa for observation and each model over the Pacific sector (110°E–120°W, 20°–75°N) in boreal winter (DJF).

EOF PC	OBS	ACCESS1-0	ACCESS1-3	BCC-CSM1-1	BCC-CSM1-1-M	CanESM2	CCSM4	CMCC-CM	CMCC-CMS	CNRM-CM5	GFDL-CM3	GFDL-ESM2G
PC1	−0.112	0.212	−0.128	−0.058	0.513	−0.155	−0.386	−0.066	0.016	−0.152	−0.103	0.1003
PC2	0.001	−0.074	−0.308	−0.243	−0.035	0.613	0.641	0.441	0.521	0.265	0.601	0.738
PC3	0.768	0.703	0.568	0.401	0.519	0.316	−0.035	0.475	0.256	0.407	−0.014	0.080
PC4	−0.117	0.062	0.180	−0.245	−0.068	−0.047	0.195	0.031	0.146	−0.336	−0.429	−0.179
		GFDL-ESM2M	HadGEM2-CC	IPSL-CM5A-LR	IPSL-CM5A-MR	IPSL-CM5B-LR	MIROC-ESM	MIROC-ESM-CHEM	MPI-ESM-LR	MPI-ESM-MR	MRI-CGCM3	NorESM1-M
PC1		0.213	0.032	0.0448	0.577	0.201	0.025	−0.270	0.648	−0.076	−0.065	0.211
PC2		0.682	0.277	−0.033	−0.126	−0.387	0.142	−0.343	0.174	0.471	0.498	0.624
PC3		−0.102	−0.215	0.512	0.246	0.408	0.655	0.043	0.301	0.280	0.319	0.066
PC4		0.110	0.046	0.444	0.271	0.389	0.006	0.667	−0.257	0.034	0.292	−0.092

and the spatial structure of North Pacific BF in Table 4 of this section, five common CMIP5 models (ACCESS1-0, ACCESS1-3, GFDL-ESM2G, IPSL-CM5A-LR, and MPI-ESM-LR), which simultaneously satisfied both objective criteria of model selection, show relatively reasonable skill in simulating the wintertime BF over the North Pacific. Thus, hereinafter, we focus on these five models and their mean to explore future changes in wintertime blocking activities over the North Pacific.

4. Changes in blocking frequency in CMIP5 models at the Pacific sector

To project the future change of the climatological characteristics in wintertime BF, the BF over the Pacific sector (110°E–120°W) is calculated using the five selected models for the historical (1975/1976–2004/2005), RCP4.5 (2070/2071–2099/2100), and RCP8.5 (2070/2071–2099/2100) simulations (Figure 4 and Table 5). In addition, the model mean values of the five simulated BFs for the historical and two RCP integrations, as well as observed BF, are described in Figure 4 and Table 5. The winter frequency of observed blocking is 5.12%. The BF of the model mean obtained from the historical simulations (5.68%) is in good agreement with that of the observation over the region. This distinct feature can be also found in Figure 1(b), whereas the BFs of the model mean from the RCP4.5 (4.69%) and 8.5 (3.74%) simulations tend to be lower compared to that obtained from the historical simulation. The BFs of all models in Figure 4, in general, show a decreasing tendency in the RCP scenario experiments, except for RCP4.5 run by ACCESS1-3. The figure shows that the two ACCESS1 models have BFs that are substantially lower than the other three models in all experiments, and that the IPSL-CM5A-LR model depicts the largest gaps (2.23% with RCP4.5 and 3.84% with RCP8.5) of the BFs between the historical and two RCP experiments. The decreasing tendency in wintertime BF under future global warming over the North Pacific region found in this study is consistent with previous results obtained using different warming scenarios, such as the Special Reports on Emission Scenarios (SRES) A2 and A1B emission scenarios in CMIP3 models (Matsueda *et al*., 2009; Woollings, 2010; Barnes *et al*., 2012). Barnes *et al.* (2012) used 14 CMIP3 general circulation models (GCMs) for both the 20C3M (1961–2000) and SRES A2 (2081–2100) scenarios to depict a robust decrease in BF with increased greenhouse gas forcing. Matsueda *et al*. (2009) used Japan Meteorological Agency (JMA)/Meteorological Research Institute (MRI) atmospheric GCMs (AGCMs) with four different resolutions, i.e. TL959L60 (20 km), TL319L60 (60 km), TL159L40 (120 km), and TL95L40 (180 km), to study the future change of wintertime atmospheric blocking in the present-day (1979–2003) and future (2075–2099) climates under the SRES A1B emission scenario. Woollings (2010) analysed the change of wintertime (DJF) blocking in the European Centre/Hamburg model version 5 (ECHAM5)/Max Planck Institute Ocean

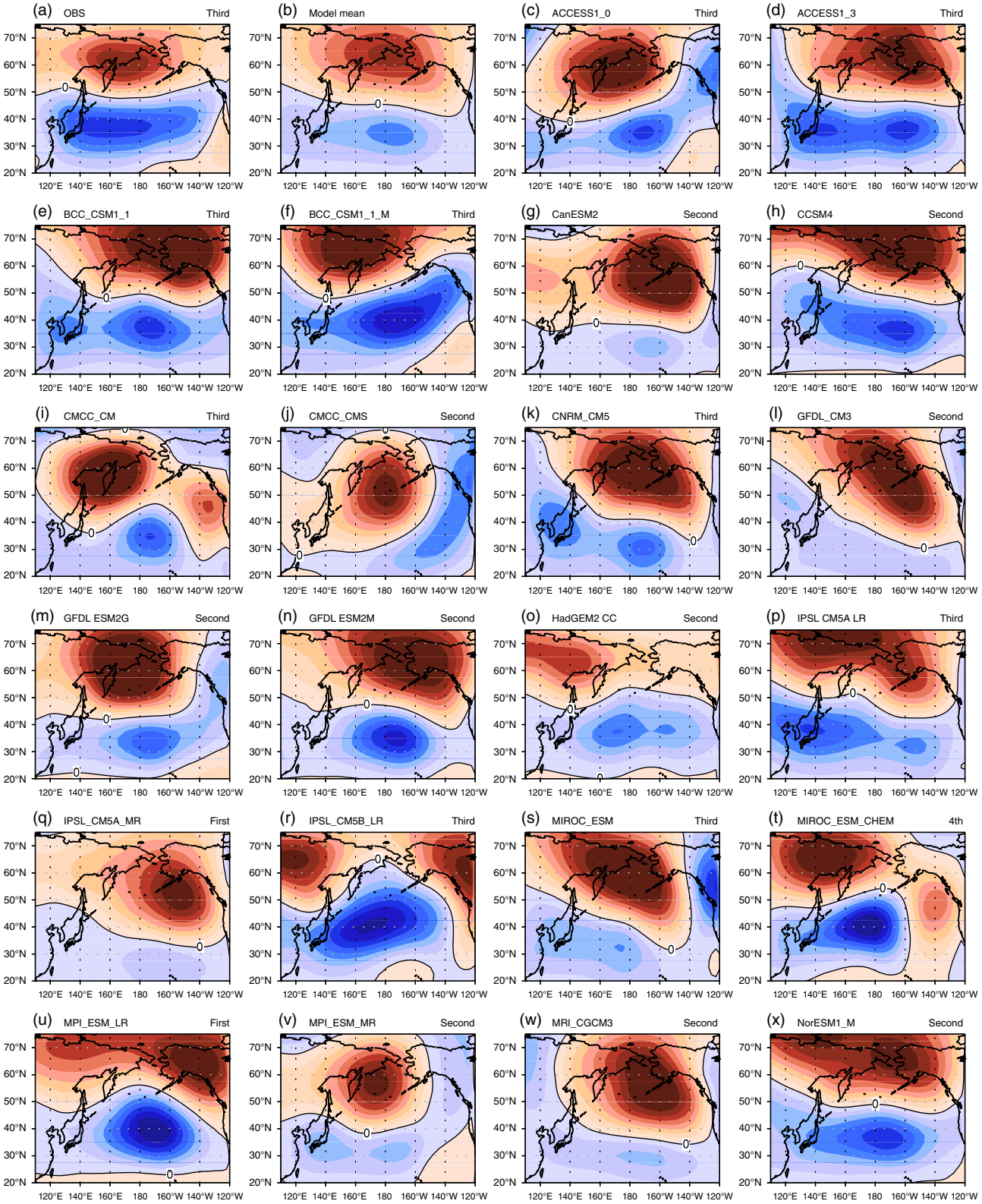

Figure 3. The spatial structures of the EOF modes of the detrended geopotential height anomaly at 500 hPa for (a) observation and (c–x) individual models derived from historical (1975/1976–2004/2005) simulations over the Pacific sector (110°E–120°W, 20°–75°N) in boreal winter (DJF) based on high correlations between wintertime blocking frequencies (BFs) and PC timeseries for observation and each model. (b) The model mean indicates the averaged spatial pattern of the EOF blocking modes of each model. The EOF modes of observation and each model are provided in the upper right. [Colour figure can be viewed at wileyonlinelibrary.com].

Table 4. Spatial PCCs (and significance test) between each model derived from the historical (1975/1976–2004/2005) simulations and observation for the spatial patterns of the EOF modes (refer to Figure 3) of the DJF detrended 500 hPa geopotential height anomalies over the Pacific sector (110°E–120°W, 20°–75°N). The asterisk (*) superscript indicates that the skill score of the model is significant at the 90% confidence level from a two-tailed Student's *t* test.

	ACCESS1-0* GFDL-ESM2M*	ACCESS1-3* HadGEM2-CC*	BCC-CSM1-1* IPSL-CM5A-LR*	BCC-CSM1-1-M* IPSL-CM5A-MR	CanESM2 IPSL-CM5B-LR	CCSM4* MIROC-ESM	CMCC-CM MIROC-ESM-CHEM*	CMCC-CMS MPI-ESM-LR*	CNRM-CM5 MPI-ESM-MR	GFDL-CM3 MRI-CGCM3	GFDL-ESM2G* NorESM1-M*
PCC (significance test)	0.756 (90%)	0.868 (95%)	0.795 (90%)	0.848 (95%)	0.502 (80%)	0.784 (90%)	0.598 (80%)	0.160 (65%)	0.685 (85%)	0.490 (75%)	0.831 (95%)
	0.781 (90%)	0.827 (90%)	0.810 (90%)	0.416 (70%)	0.632 (85%)	0.681 (85%)	0.729 (90%)	0.716 (90%)	0.705 (85%)	0.484 (75%)	0.888 (95%)

Model (MPI-OM) CGCM, using simulations from the CMIP3 archive for the 20th century (20C3M) and 21st century (SRES A1B).

Figure 5 shows the climatological BF as a function of duration for observation and model simulations over the Pacific sector (110°E–120°W) during DJF. To examine the biases of BF for historical simulations against observation and potential future changes of BF for RCP4.5 and 8.5 simulations against historical simulations, the relative differences of BF duration for each simulation are also calculated (Figure 5(d)–(f)). In general, the BFs in all five CMIP5 models exhibit an exponential decrease with duration. The historical simulations of both ACCESS1-0 and ACCESS1-3 tend to underestimate the frequency of short-lived Pacific blocking of a duration shorter than 8–9 days, as compared to the observed BF (Figure 5(a) and (b)), whereas the frequency distributions of Pacific blocking of almost all durations simulated by the GFDL-ESM2G, IPSL-CM5A-LR, and MPI-ESM-LR in the present climate tend to be overestimated (Figure 5(c) and (e)). The Pacific BF of the model mean from historical simulations, showing a BF difference of <1% in all durations, has a similar distribution to that of the observation (Figure 5(f)). Compared with the historical simulations by each model as well as the model mean, all RCP simulations in the future climate, except for RCP4.5 run by ACCESS1-3, project a reduction in the Pacific BF for almost all durations. Furthermore, the RCP8.5 simulations show more clearly a decrease in Pacific BF compared to the RCP4.5, especially in a duration shorter than 9–10 days.

It is well known that atmospheric blocking is a phenomenon characterized by reduction of the strength of the westerly zonal flows (Rex, 1950; Matsueda *et al*., 2009, 2010). In Figures 6 and 7, we examine whether the changes of winter BF can be explained through changes of the zonal flow and its variability in response to greenhouse gas forcing. Figure 6 and Table 5 present climatological mean zonal wind speed at the 250 hPa level, area-averaged (150°E–150°W, 25°–45°N) over the Pacific region during DJF, obtained from the observation and the five CMIP5 models for the historical and two RCP scenario experiments for the period of 30 years. The five-model mean zonal wind speeds for the three experiments are also shown in the same figure and table. The observations show relatively large standard deviations (green bars) in wind speed distribution. Generally, an increase of the zonal wind speed is accompanied by a decrease in the frequency of blocking events. The speeds of the mid-latitude upper level zonal wind derived from each model and model mean in Figure 6 and Table 5 depict the increasing trend in the RCP scenario experiments well. The historical simulations of ACCESS1-0, ACCESS1-3 and IPSL-CM5A-LR slightly overestimate the upper level zonal wind speed as compared to observations, while the other two historical simulations depict the relatively weak zonal wind speeds.

To further examine the change of spatial patterns for wintertime 250 hPa zonal winds from the five models under the historical and RCP experiments, we examine the bias and future change from the model means (Figure 7). In the

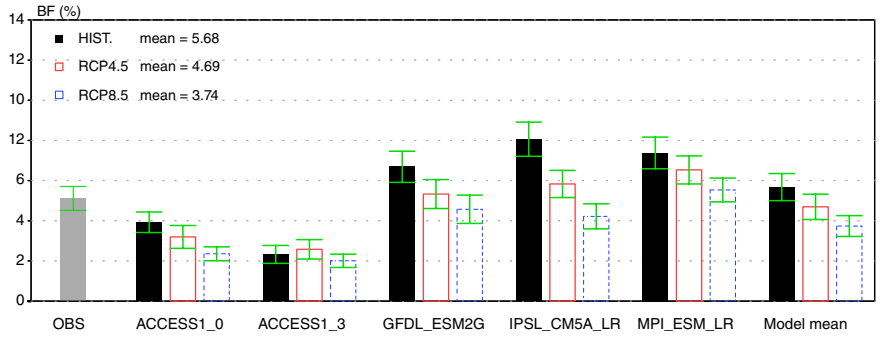

Figure 4. Climatology of the BF (unit: %) for observation, the best five models, and the model mean over the Pacific sector (110°E–120°W) in boreal winter (DJF). The grey bar indicates the observed BF (1975/1976–2004/2005). The black, red, and blue bars represent the BF derived from the historical (1975/1976–2004/2005), RCP4.5 (2070/2071–2099/2100), and RCP8.5 (2070/2071–2099/2100) simulations, respectively. The green (I) bars are centred on the mean, and the upper and lower ends indicate ±1 S.D. from the mean, respectively. [Colour figure can be viewed at wileyonlinelibrary.com].

Table 5. Climatological BF (unit: %), area-averaged zonal wind at 250 hPa (unit: m s^{-1}, area: 25°–45°N, 150°E–150°W) and differences in 1000–250 hPa thickness (unit: m) between two regions (40°–50°N and 15°–25°N in 150°E–150°W) in the Pacific sector (110°E–120°W) for boreal winter (DJF). Refer to Section 4 for more details related to each value.

	BF (unit: %)			250 hPa zonal wind (unit: m s^{-1})			1000–250 hPa thickness differences (unit: m)		
	HIST	RCP4.5	RCP8.5	HIST	RCP4.5	RCP8.5	HIST	RCP4.5	RCP8.5
Observation	5.12			44.3			810.8		
ACCESS1-0	3.93	3.20	2.36	44.5	46.7	47.8	858.7	900.0	922.2
ACCESS1-3	2.33	2.58	2.01	46.6	47.7	49.3	902.1	927.1	964.1
GFDL-ESM2G	6.69	5.33	4.57	41.6	44.0	45.9	863.8	900.6	938.2
IPSL-CM5A-LR	8.06	5.83	4.22	50.8	51.9	55.6	970.0	994.8	1070.9
MPI-ESM-LR	7.38	6.53	5.53	41.1	41.9	46.1	783.6	799.9	873.3
Model mean	5.68	4.69	3.74	44.9	46.4	48.9	875.6	904.5	953.7

historical simulation mean, a negative bias is shown over the Pacific sector. The two model-mean RCP simulations project stronger westerly wind patterns in the Pacific sector than the historical simulation. Figures 4–7 show that the climatological winter BF and upper level zonal wind over the Pacific region will decrease and increase, respectively, in the future based on the projection of the models. Several previous studies also mentioned a similar relationship between the two variables in model simulations (Matsueda *et al*., 2009, 2010; Woollings, 2010; Barnes and Polvani, 2013; de Vries *et al*., 2013; Dunn-Sigouin and Son, 2013).

To further understand the change of the strength in upper level zonal wind over the Pacific area in the future climate, the change of thickness gradient, which is proportional to the change of the upper level zonal wind, is investigated. The future change of upper level zonal flow at mid-latitude is examined using differences in 1000–250 hPa thickness between two meridional areas, 40°–50°N and 15°–25°N of 150°E–150°W, as shown in Figure 8 and Table 5. Observed climatological wintertime 1000–250 hPa thickness difference is about 811 m (Table 5). Most models, except for the MPI-ESM-LR (around 784 m), overestimate the meridional thickness differences in the historical simulations as compared with the observations. The meridional thickness gradients for all models and model means show an increasing tendency in the warmer climate, which is consistent through thermal wind balance with the trend of upper level zonal wind in Figure 6, as compared to the present climate.

Many studies (Lorenz and DeWeaver, 2007; Lu *et al*., 2007; Vecchi and Soden, 2007; Gastineau *et al*., 2008, 2009; Levine and Schneider, 2011) have tried to diagnose the changes in extension and intensity of the Hadley circulation using a variety of atmospheric variables in the scenario simulations of global warming. The change in the Hadley circulation may affect the mid-latitude zonal wind through the changes of the meridional temperature gradient as well as the meridional transport of zonal angular momentum. In this study, the meridional extension and intensity of the Hadley circulation over the Pacific region in the future climate are also examined using the climatological zonal wind and velocity potential at 250 hPa for the five-model mean derived from the historical and two RCP simulations (Figure 9). By diagnosing the changes of the Hadley circulation, we examine a possible relationship between the strengthened upper-level zonal flow and the decreasing trend of BF over the Pacific in the warm climate. From the difference between RCPs and historical simulations of the 250 hPa zonal wind in Figure 9(a) and (b), the enhancement and northward shift of the upper-level zonal wind can be found under global warming conditions. Following Levine and Schneider (2011), the extent of the Hadley circulation is estimated by calculating the latitude at which the climatological

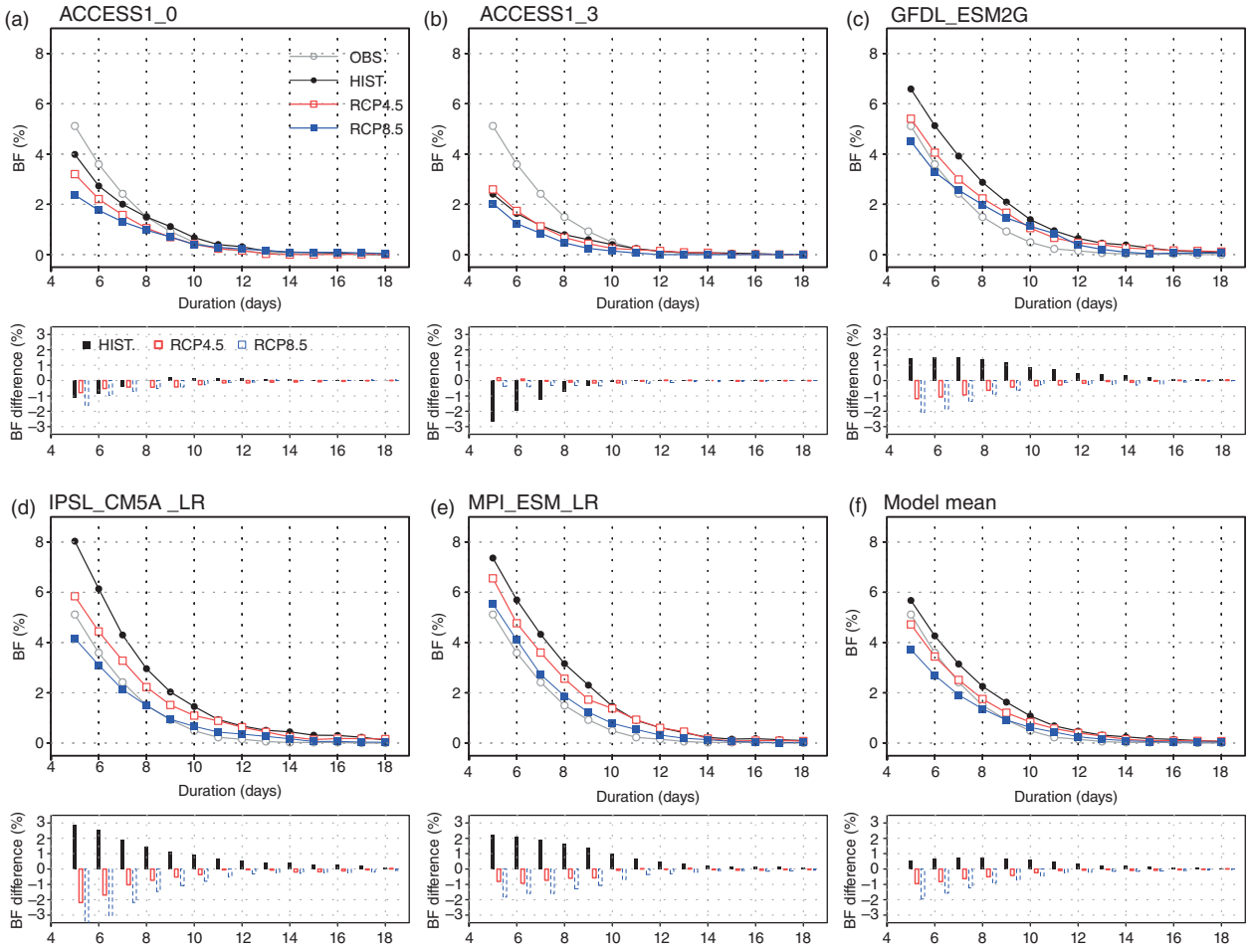

Figure 5. Climatological winter (DJF) BF (unit: %) and its difference as a function of duration over the Pacific sector (110°E–120°W) in (a–e) each model and (f) the model mean. BF difference for the historical simulation indicates bias against observation, and BF difference for the RCP4.5 or RCP8.5 simulation shows future change against historical simulation. The grey, black, red, and blue lines (or bars) denote BFs (or its differences) for observation, historical (1975/1976–2004/2005), RCP4.5 (2070/2071–2099/2100), and RCP8.5 (2070/2071–2099/2100) simulations, respectively. [Colour figure can be viewed at wileyonlinelibrary.com].

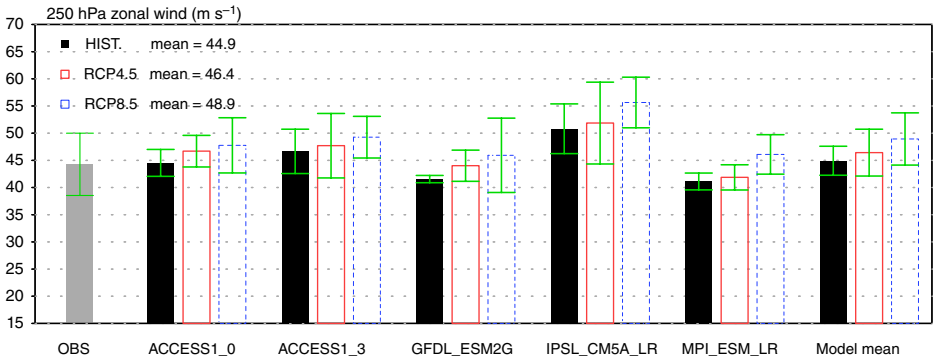

Figure 6. Climatological area-averaged zonal winds at 250 hPa (U250, unit: m s^{-1}) over the area 150°E–150°W, 25°–45°N for observation, each of the five models, and the model mean in DJF. The grey bar indicates the observed U250 (1975/1976–2004/2005). The black, red, and blue bars represent U250 derived from the historical (1975/1976–2004/2005), RCP4.5 (2070/2071–2099/2100), and RCP8.5 (2070/2071–2099/2100) simulations, respectively. The green bars are centred on the mean and span from ±1 S.D. [Colour figure can be viewed at wileyonlinelibrary.com].

zonal wind at 250 hPa in the Pacific region (150°E–180°) has the maximum wind speed. As shown in Figure 9(e), along with the increase in the model mean maximum westerly wind speed at 250 hPa in the RCP simulations, the response of the upper-level maximum zonal wind to global warming generally shows a northward shift over the Pacific region during winter, although the directions of the shift for the some models are not clear (figure not shown). Furthermore, the strengthened divergence field of climatological upper-level velocity potential over the

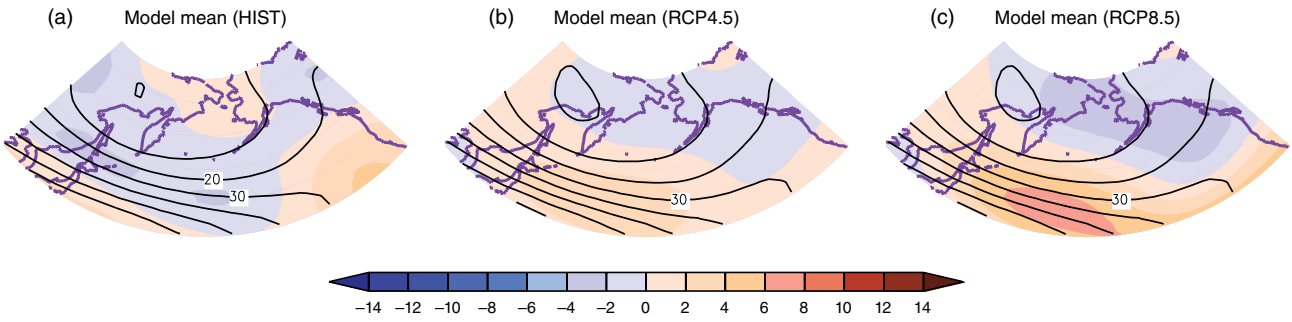

Figure 7. (a) Bias for the model mean of the historical simulations against observation (1975/1976–2004/2005) and (b–c) future change for the model mean of the RCP simulations (2070/2071–2099/2100) against historical simulation (1975/1976–2004/05) for wintertime climatological 250 hPa zonal wind (U250, unit: m s^{-1}) over the Pacific region (120°E–120°W, 35°–70°N). The contour line in (a) (b and c) indicates climatological DJF mean U250 for observation (historical model mean). [Colour figure can be viewed at wileyonlinelibrary.com].

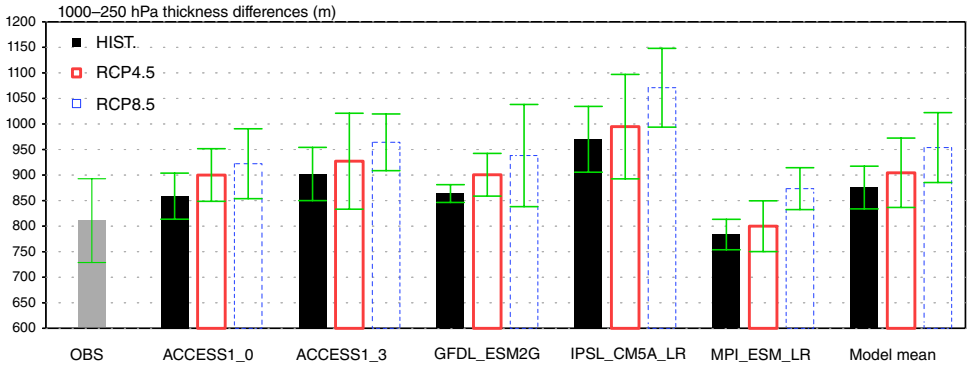

Figure 8. Climatological mean differences in 1000–250 hPa thickness (unit: m) between two regions 40°–50°N and 15°–25°N in 150°E–150°W of the Pacific region in boreal winter (DJF). The grey bar indicates the observed mean thickness difference (1975/1976–2004/2005). The black, red, and blue bars represent estimates of mean thickness differences derived from the historical (1975/1976–2004/2005), RCP4.5 (2070/2071–2099/2100), and RCP8.5 (2070/2071–2099/2100) simulations, respectively. The green bars are centred on the mean and span from ±1 S.D. [Colour figure can be viewed at wileyonlinelibrary.com].

Equator to 30°N in Figure 9(c), (d), and (f) implies a high probability of the poleward shift of the Hadley circulation under global warming. The divergence field core over the maritime continent (Figure 9(c) and (d)) and strength of the zonal mean (150°E–180°) upper-level velocity potential near 10°S (Figure 9(f)) tend to decrease in the future climate against the present climate. These results show that the Hadley circulation strength weakens in the future climate as compared with the present climate, and the future changes in Hadley circulation strength for all five models are also individually consistent with those for the model mean (figure not shown). Many previous studies (Mitas and Clement, 2006; Lu *et al*., 2007; Gastineau *et al*., 2008) also presented a poleward extension of the Hadley circulation area accompanied by weakening of the circulation intensity in the scenario simulation of global warming. The main factor leading to the enhancement of the upper-level zonal wind is the increased meridional temperature gradients associated with the expansion of the Hadley cell, consistent with the overall decrease in the BF over the Pacific sector in the warmer climate. The effect of angular momentum conservation in decreasing the zonal wind related to the weakened Hadley circulation (weak divergence field near 10°S under warm conditions) appears to be much weaker than the influence of the increased meridional temperature gradient under global warming condition of the future climate.

5. Changes in blocking intensity in the Pacific sector in CMIP5 models

In this section, the climatological BI is analysed to diagnose the relative strength of large-scale zonal flow in blocking regions (more details are described in Section 2.3; Wiedenmann *et al*., 2002) using the five models derived from the historical (1975/1976–2004/2005) and two RCP (2070/2071–2099/2100) simulations over the Pacific sector (110°E–120°W, 35°–70°N) in boreal winter (DJF) for 30-year periods (Figure 10 and Table 6). Observed BI and the averaged BIs of the five models for each simulation are calculated for the same period (Figure 10 and Table 6). The climatological BIs of the two ACCESS1 models (both are about 2.20) obtained from the historical simulations over the Pacific region are similar to that of the observation (2.26). However, the climatological BIs of other models from the historical simulations are slightly stronger than that obtained from observation. Consequently, the averaged intensity of climatological blocking of the model mean displays a relatively larger value than the observed BI, but the difference is not statistically significant according to a *t*-statistic. Overall,

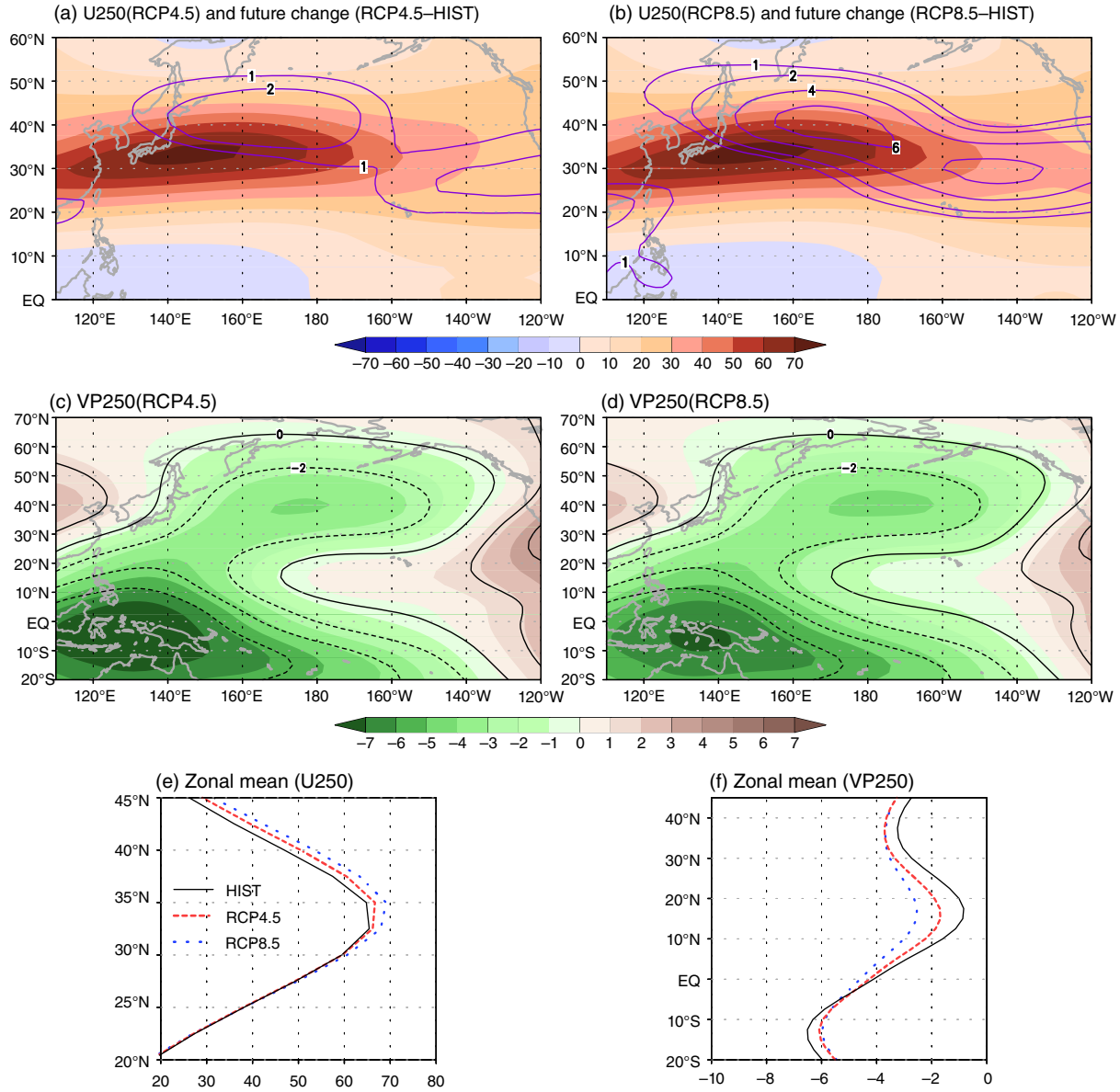

Figure 9. (a–d) Climatology and (e–f) zonal mean (150°E–180°) for (a, b, and e) zonal wind (unit: m s^{-1}) and (c, d, and f) velocity potential (unit: 10^6 m^2 s^{-1}) at 250 hPa during winter (DJF) for the model mean derived from the historical (1975/1976–2004/2005, black line), RCP4.5 (2070/2071–2099/2100, red line), and RCP8.5 (2070/2071–2099/2100, blue line) simulations, respectively. The contours (unit: m s^{-1}, purple) in (a) and (b) indicate the difference between RCPs and historical simulation for 250 hPa zonal wind. The black lines in (c) and (d) represent climatological velocity potential obtained from historical simulation. [Colour figure can be viewed at wileyonlinelibrary.com].

the climatological wintertime BIs derived from the RCP simulations as the warmer climate in the Pacific sector show a weakening tendency compared to those obtained from historical simulations, although some of the selected models, such as two ACCESS1 and GFDL-ESM2G, do not show a decreasing trend more clearly; especially in the model mean and two CMIP5 models of IPSL-CM5A-LR and MPI-ESM-LR, the trend of reduction is stronger. These findings generally coincide with the decreasing tendency in climatological wintertime BF over the North Pacific region under global warming conditions. For reference, we also found a consistent decreasing trend across the mean values of climatological BI for the whole 22 model set, and, in particular, seven out of them had a clear decreasing tendency (figure not shown).

To examine the climatological characteristics of the BI distribution, we compute the number of blocking events and their probability as a function of BI for observation and model simulations, including the model mean over the Pacific sector (110°E–120°W) during boreal winter in the present and future climate (Figure 11). BI is classified from an intensity 'bin' 0–5, at intervals of 0.5, where 'bin' 0 represents events of BI from 0.0 to 0.5 ($0.0 \leq \mathrm{BI} < 0.5$). In each model, the probability of blocking events denotes the statistical number of each blocking event with a given intensity divided by the total number of blocking events in each climate scenario (i.e. the total area under the curve for a given scenario in the top panels of Figure 11(a)–(f)). The distributions of blocking events with BI in the five selected models from the historical and RCP simulations

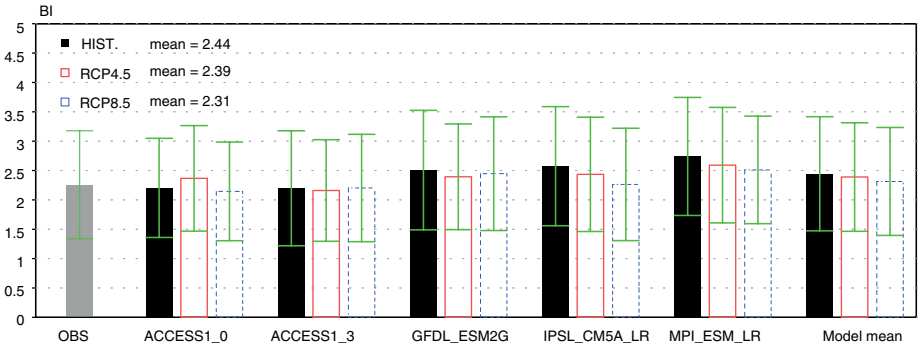

Figure 10. Climatology of the BI for observation, each of the five models, and the model mean over the Pacific sector (110°E–120°W, 35°–70°N) in boreal winter (DJF). The grey bar indicates the observed BI (1975/1976–2004/2005). The black, red, and blue bars represent the BI derived from the historical (1975/1976–2004/2005), RCP4.5 (2070/2071–2099/2100), and RCP8.5 (2070/2071–2099/2100) simulations, respectively. The green bars are centred on the mean and span from ±1 S.D. [Colour figure can be viewed at wileyonlinelibrary.com].

Table 6. Climatological BI for observation, each of the five models, and the model mean over the Pacific sector (110°E–120°W, 35°–70°N) in boreal winter (DJF)

	Observation	ACCESS1-0	ACCESS1-3	GFDL-ESM2G	IPSL-CM5A-LR	MPI-ESM-LR	Model mean
HIST	2.26	2.20	2.20	2.51	2.57	2.74	2.44
RCP4.5		2.37	2.16	2.39	2.44	2.59	2.39
RCP8.5		2.15	2.20	2.45	2.26	2.51	2.31

and their model mean values are similar to the distribution patterns (with the maximum values between BIs from 1.5 to 2.5) of occurrence number and probability of the observed blocking events. For the model mean, the number of events in terms of BI in the historical simulation differs substantially between bins 1 and 3 (BI from 1.0 to 3.5), as compared to those in the RCP simulations. However, a large gap does not appear for the probability of blocking events. The probabilities of strong intensity of more than bin 3 in the future climate tend to decrease slightly compared to those in the present climate, while the probabilities of blocking events in the future climate with weak intensity of less than bin 1 show a tendency to slightly increase.

Based on the average and standard deviation of the BI for observation and the model mean, we first calculate the classification criteria to find the cause of the future trend of climatological BI through the probability distribution of intensity of the blocking events. The probability distribution of BI is classified into three categories: 'weak', 'moderate', and 'strong', defined as the probability of the events weaker than bin 1, between bin 1 and bin 3, and stronger than bin 3, respectively, using the criteria of BI (Table 7). The probability of strong BI (17.27%) of the model mean in the present climate shows a bias about twice that of the observation (9.17%) and has a decreasing tendency under global warming conditions. For blocking events with weak intensity, the probability (4.49%) of the model mean from the historical simulation is about half of the occurrence probability of the observation (8.52%). The probability of weak BI in the RCP simulations indicates a gradual increasing trend in comparison with that in the historical simulation. Furthermore, the future trend of strong BI, unlike weak or moderate BI, which shows an increasing trend in the warmer climate, is similar to the general decreasing tendency of climatological BI in Figure 10. This indicates that the future change of occurrence of blocking events with strong intensity may have a great effect on the future trend of total climatological BI over the Pacific sector in boreal winter. Figure 11 and Table 7 illustrate that the opposite-signed trends in probability for different BI in the future are the results obtained from the contribution to the total number of BI events in each global warming condition by the definition of the probability, not indicating the trends of the number of blocking events in the categories of BI.

6. Summary and conclusions

In this study, the change of BF and BI for winter in response to global warming is investigated using the historical and two RCP simulations in the CMIP5 coupled models, which are chosen on the basis of the availability of data such as daily geopotential height and zonal wind from each model simulation.

We focus on the North Pacific sector, which reproduces the climatological features of BF reasonably well in the historical simulations of the CMIP5 models. Using the distinct features in the dominant variability and spatial structure of BF over the North Pacific, the five best CMIP5 models (ACCESS1-0, ACCESS1-3, GFDL-ESM2G, IPSL-CM5A-LR, and MPI-ESM-LR) are selected to explore the future changes in wintertime Pacific blocking activities.

The investigation of the future change of the climatological features in Pacific BF for winter reveals that the

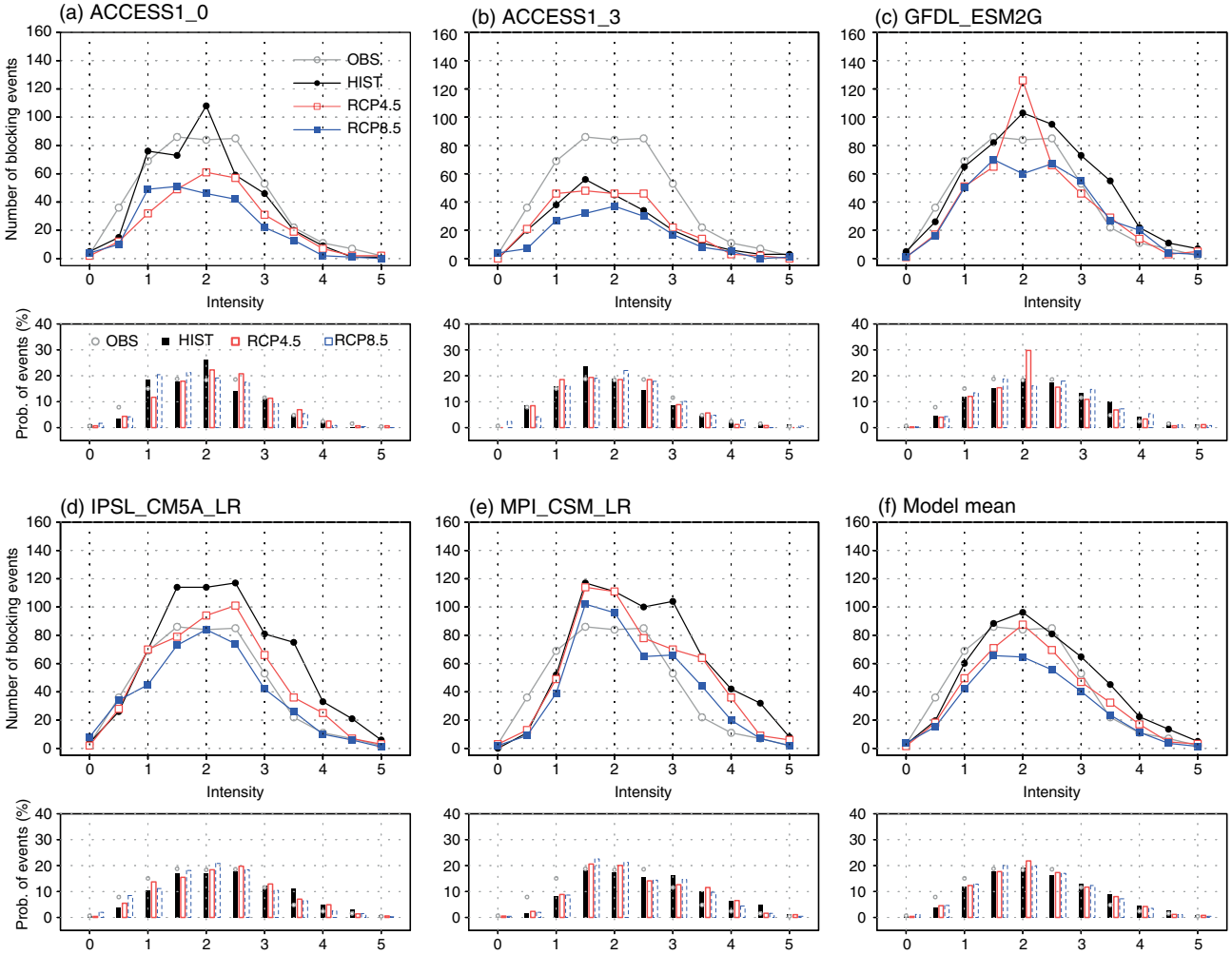

Figure 11. Number and probability of blocking events as a function of BI for (a–e) each model and (f) the model mean over the Pacific sector (110°E–120°W) in boreal winter. Each number of the *x*-axis indicates an intensity 'bin' at intervals of 0.5 (e.g. 1 represents events of BI, $1.0 \leq \mathrm{BI} < 1.5$). The probability of events shows the rate calculated by the number of each BI event divided by the total number of BI events in each climate change scenario. The grey, black, red, and blue lines (or bars) denote values for observation, historical (1975/1976–2004/2005), RCP4.5 (2070/2071–2099/2100), and RCP8.5 (2070/2071–2099/2100) simulations, respectively. [Colour figure can be viewed at wileyonlinelibrary.com].

Table 7. Probability distribution of the BI for observation and the model mean in climate change scenarios through three categories (where 'weak', 'moderate', and 'strong' represent the probability of the events weaker than bin 1, between bin 1 and bin 3, and stronger than bin 3, respectively) based on the average and S.D. of the BI.

		Average of BI	S.D. of BI	Probability of the BI		
				Weak (%)	Moderate (%)	Strong (%)
OBS		2.26	0.92	8.52	55.68	9.17
Model mean	HIST	2.44	0.97	4.49	53.21	17.27
	RCP4.5	2.39	0.93	4.93	56.69	14.19
	RCP8.5	2.31	0.92	5.81	56.78	12.22

BFs of most models and their model mean values in the warmer climate decrease, as compared to the historical simulation, as has been previously reported (Matsueda *et al*., 2009; Barnes *et al*., 2012; Dunn-Sigouin and Son, 2013). For the change of BF with duration, all five models depict an exponentially decreasing pattern in the historical and two RCP scenario experiments. In particular, the decreasing future changes in the frequency of short-lived (<9–10 days) Pacific blocking for each simulation of all five models are much more noticeable than those in long-lived (>10 days) Pacific BF.

Through the change of main features of the upper-level zonal wind in the warmer climate, it is found that the upper-level westerly wind exhibits an increase of speed and stronger eastward pattern, as opposed to the decreasing tendency in BF. To investigate the possible causes of this future change in the upper-level zonal flow under global warming conditions, we diagnose the difference

of thickness in the layer of 1000–250 hPa between two meridional regions at mid-latitude and also check the future change in the Hadley circulation strength and extension over the subtropical region. We find that the strengthened upper-level westerly wind, leading to less meandering flow, consistent with the enhanced meridional temperature gradients, has a very strong relationship with the decreasing tendency of Pacific BF in the future climate. In addition, our use of model mean values to investigate the future trend of Hadley circulation reveals the existence of a poleward extension of Hadley circulation (the Equator to 30°N) related with the enhancement of the zonal upper-level wind as well as the weakening intensity of Hadley cell (20°S to the Equator) over the Pacific region in response to global warming. These results indicate that the strengthened upper-level westerly and northward extension of the Hadley cell arise from the enhancement of the meridional thickness gradients. As compared with the effect of angular momentum conservation in weakening the zonal wind and Hadley circulation caused by the weakened upper-level divergence field in the future climate, the meridional temperature gradient strengthened from global warming appears to have a much stronger influence.

From the future changes in climatological BI distribution, it is found that the future trend of reduced climatological winter BI for the model mean may be closely linked to the deceasing tendency in the probability of the occurrence of blocking events with strong intensity.

This research, based on the ability to simulate blocking in the CMIP5 historical experiments, has predicted how the future trends of BF and BI change under the global warming conditions and has investigated the main factors that contribute to these results. Although the data and/or blocking detection method used in this study differs from those of previous studies, the reduction tendencies in the wintertime North Pacific blocking climatology derived from the RCP simulations are similar to those previously reported (Matsueda *et al*., 2009; Barnes *et al*., 2012; Dunn-Sigouin and Son, 2013).

Most of the models tend to have quite large model biases in wintertime blocking climatology over the North Pacific in the CMIP5 historical simulations. Further studies aimed at more accurately predicting the change of blocking climatology in the future will need to exert more diverse efforts to reduce model biases in blocking (Matsueda *et al*., 2009; Scaife *et al*., 2010, 2011; Anstey *et al*., 2013). A consequent improvement of model biases may enable the prediction of not only the blocking events but also the various climate phenomena of the near future with accuracy sufficient to support a quick response to future climate changes.

Acknowledgements

This work was funded by the Korea Meteorological Administration Research and Development Program under grant KMIPA 2015-2081.

References

Anstey JA, Davini P, Gray LJ, Woollings T, Butchart N, Cagnazzo C, Christiansen B, Hardiman SC, Osprey SM, Yang S. 2013. Multi-model analysis of Northern Hemisphere winter blocking: model biases and the role of resolution. *J. Geophys. Res.* **118**: 3956–3971, doi: 10.1002/jgrd.50231.

Barnes EA, Hartmann DL. 2010. Influence of eddy-driven jet latitude on North Atlantic jet persistence and blocking frequency in CMIP3 integrations. *Geophys. Res. Lett.* **37**: L23802, doi: 10.1029/2010GL045700.

Barnes EA, Polvani L. 2013. Response of the midlatitude jets, and of their variability, to increased greenhouse gases in the CMIP5 models. *J. Clim.* **26**(18): 7117–7135, doi: 10.1175/JCLI-D-12-00536.1.

Barnes EA, Slingo J, Woollings T. 2012. A methodology for the comparison of blocking climatologies across indices, models and climate scenarios. *Clim. Dyn.* **38**: 2467–2481.

Barriopedro D, García-Herrera R, Lupo AR, Hernandez E. 2006. A climatology of Northern Hemisphere blocking. *J. Clim.* **19**: 1042–1063.

Barriopedro D, Garcı´a-Herrera R, Huth R. 2008. Solar modulation of Northern Hemisphere winter blocking. *J. Geophys. Res.* **113**: D14118, doi: 10.1029/2008JD009789.

Berckmans J, Woollings T, Demory ME, Vidale PL, Roberts M. 2013. Atmospheric blocking in a high resolution climate model: influences of mean state, orography and eddy forcing. *Atmos. Sci. Lett.* **14**: 34–40.

Black E, Blackburn M, Harrison G, Hoskins B, Methven J. 2004. Factors contributing to the summer 2003 European heatwave. *Weather* **59**: 217–223.

Buehler T, Raible CC, Stocker TF. 2011. The relationship of winter season North Atlantic blocking frequencies to extreme cold or dry spells in the ERA-40. *Tellus* **63A**: 212–222.

Cheung HN, Zhou W, Mok HY, Wu MC, Shao Y. 2013. Revisiting the climatology of atmospheric blocking in the Northern Hemisphere. *Adv. Atmos. Sci.* **30**(2): 397–410, doi: 10.1007/s00376-012-2006-y.

D'Andrea F, Tibaldi S, Blackburn M, Boer G, Déqué M, Dix M, Dugas B, Ferranti L, Iwasaki T, Kitoh A, Pope V, Randall D, Roeckner E, Strauss D, Stem W, Van den Dool H, Williamson D. 1998. Northern Hemisphere atmospheric blocking as simulated by 15 atmospheric general circulation models in the period 1979–1988. *Clim. Dyn.* **14**: 385–407.

Dole R, Hoerling M, Perlwitz J, Eischeid J, Pegion P, Zhang T, Quan X-W, Xu T, Murray D. 2011. Was there a basis for anticipating the 2010 Russian heat wave? *Geophys. Res. Lett.* **38**: L06702, doi: 10.1029/2010GL046582.

Dunn-Sigouin E, Son S-W. 2013. Northern Hemisphere blocking frequency and duration in the CMIP5 models. *J. Geophys. Res. Atmos.* **118**: 1179–1188, doi: 10.1002/jgrd.50143.

Gastineau G, Li K, Treut H, Li L. 2008. Hadley circulation changes under global warming conditions indicated by coupled climate models. *Tellus* **60A**: 863–884.

Gastineau G, Li K, Treut H. 2009. The Hadley and Walker circulation changes in global warming conditions described by idealized atmospheric simulations. *J. Clim.* **22**: 3993–4013, doi: 10.1175/2009JCLI2794.1.

Gruza GV, Korovkina LV. 1991. Seasonal features of spatial distribution of blocking indices in the Northern Hemisphere. *Meteor. Hydrol.* **3**: 108–110.

Jolliffe IT, Stephenson DB. 2003. *Forecast Verification: A Practitioner's Guide in Atmospheric Science*. John Wiley & Sons, Ltd: Chichester, West Sussex, England, ISBN: 0-471-49759-2.

Kalnay E, Kanamitsu M, Kistler R, Collins W, Deaven D, Gandin L, Iredell M, Saha S, White G, Woollen J, Zhu Y, Leetmaa A, Reynolds B, Chelliah M, Ebisuzaki W, Higgins W, Janowiak J, Mo KC, Ropelewski C, Wang J, Jenne R, Joseph D. 1996. The NCEP/NCAR 40-year reanalysis project. *Bull. Am. Meteorol. Soc.* **77**: 437–470.

Lejenas H, Okland H. 1983. Characteristics of Northern Hemisphere blocking as determined from a long time series of observational data. *Tellus* **35A**: 350–362.

Levine XJ, Schneider T. 2011. Response of the Hadley circulation to climate change in an aquaplanet GCM coupled to a simple representation of ocean heat transport. *J. Atmos. Sci.* **68**: 769–783, doi: 10.1175/2010JAS3553.1.

Lorenz DJ, DeWeaver ET. 2007. Tropopause height and zonal wind response to global warming in the IPCC scenario integrations. *J. Geophys. Res.* **112**: D10119, doi: 10.1029/2006JD008087.

Lu J, Vecchi GA, Reichler T. 2007. Expansion of the Hadley cell under global warming. *Geophys. Res. Lett.* **34**: L06805, doi: 10.1029/2006GL028443.

Lupo AR, Smith PJ. 1995. Climatological features of blocking anticyclones in the Northern Hemisphere. *Tellus* **47A**: 439–456.

Masato G, Hoskins BJ, Woollings T. 2013. Winter and summer Northern Hemisphere blocking in CMIP5 models. *J. Clim.* **26**: 7044–7059.

Matsueda M, Mizuta R, Kusunoki S. 2009. Future change in wintertime atmospheric blocking simulated using a 20-km-mesh atmospheric global circulation model. *J. Geophys. Res.* **114**: D12114, doi: 10.1029/2009JD011919.

Matsueda M, Endo H, Mizuta R. 2010. Future change in Southern Hemisphere summertime and wintertime atmospheric blockings simulated using a 20-km-mesh AGCM. *Geophys. Res. Lett.* **37**: L02803, doi: 10.1029/2009GL041758.

Mitas CM, Clement A. 2006. Recent behavior of the Hadley cell and tropical thermodynamics in climate models and reanalyses. *Geophys. Res. Lett.* **33**: L01810, doi: 10.1029/2005GL024406.

Mokhov II, Timazhev AV, Lupo AR. 2014. Changes in atmospheric blocking characteristics within the EuroAtlantic region and Northern Hemisphere as a whole in the 21st century in models using RCP anthropogenic scenarios. *Global Planet. Change* **122**: 265–270.

Nakamura H. 1994. Rotational evolution of potential vorticity associated with a strong blocking flow configuration over Europe. *Geophys. Res. Lett.* **21**: 2003–2006.

Neiman PJ, Persson POG, Ralph FM, Jorgensen DP, White AB, Kingsmill DE. 2004. Modification of fronts and precipitation by coastal blocking during an intense landfalling winter storm in Southern California: observations during CALJET. *Mon. Weather Rev.* **132**: 242–273.

Park Y-J, Ahn J-B. 2014. Characteristics of atmospheric circulation over East Asia associated with summer blocking. *J. Geophys. Res. Atmos.* **119**: 726–738, doi: 10.1002/2013JD020688.

Park T-W, Ho C-H, Yang S. 2011. Relationship between the arctic oscillation and cold surges over East Asia. *J. Clim.* **24**: 68–83.

Rex DF. 1950. Blocking action in the middle troposphere and its effect on regional climate II: the climatology of blocking action. *Tellus* **3**: 275–301.

Scaife AA, Woollings T, Knight JR, Martin G, Hinton T. 2010. Atmospheric blocking and mean biases in climate models. *J. Clim.* **23**: 6143–6152, doi: 10.1175/2010JCLI3728.1.

Scaife AA, Copsey D, Gordon C, Harris C, Hinton T, Keeley S, O'Neill A, Roberts M, Williams K. 2011. Improved Atlantic winter blocking in a climate model. *Geophys. Res. Lett.* **38**: L23703, doi: 10.1029/2011GL049573.

Tanaka HL, Milkovich MF. 1990. A heat budget analysis of the polar troposphere in and around Alaska during the abnormal winter of 1988/89. *Mon. Weather Rev.* **118**: 1628–1639.

Taylor K, Stouffer R, Meehl G. 2012. An overview of CMIP5 and the experiment design. *Bull. Am. Meteorol. Soc.* **93**: 485–498.

Tibaldi S, Molteni F. 1990. On the operational predictability of blocking. *Tellus* **42A**: 343–365.

Tibaldi S, Tosi E, Navarra A, Pedulli L. 1994. Northern and Southern Hemisphere seasonal variability of blocking frequency and predictability. *Mon. Weather Rev.* **122**: 1971–2003.

Triedl RA, Birch EC, Sajecki P. 1981. Blocking action in the Northern Hemisphere: a climatological study. *Atmos.–Ocean* **19**: 1–23.

Vecchi GA, Soden BJ. 2007. Global warming and the weakening of the tropical circulation. *J. Clim.* **20**: 4316–4340.

Vial J, Osborn TJ. 2012. Assessment of atmosphere–ocean general circulation model simulations of winter Northern Hemisphere atmospheric blocking. *Clim. Dyn.* **39**: 95–112.

de Vries H, Woollings T, Anstey J, Haarsma RJ, Hazeleger W. 2013. Atmospheric blocking and its relation to jet changes in a future climate. *Clim. Dyn.* **41**(9–10): 2643–2654.

Wiedenmann JM, Lupo AR, Mokhov II, Tikhonova E. 2002. The climatology of blocking anticyclones for the Northern and Southern Hemispheres: block intensity as a diagnostic. *J. Clim.* **15**: 3459–3473.

Woollings T. 2010. Dynamical influences on European climate: an uncertain future. *Phil. Trans. R. Soc. A* **368**: 3733–3756, doi: 10.1098/rsta.2010.0040.

World Meteorological Organization. 2006. Standardised verification system (SVS) for long-range forecasts (LRF): new attachment II-8 to the manual on the GDPFS. WMO 485, vol. I, 83 pp., Geneva, Switzerland.

You J-E, Ahn J-B. 2012. The anomalous structures of atmospheric and oceanic variables associated with the frequency of North Pacific winter blocking. *J. Geophys. Res.* **117**: D11108, doi: 10.1029/2012JD017431.